

1 **Secondary Organic Aerosols from OH Oxidation of Cyclic Volatile Methyl Siloxanes as an Important**
2 **Si Source in the Atmosphere**

3 Chong Han^{1,2}, Hongxing Yang¹, Kun Li^{2,3}, Patrick Lee², John Liggi², Amy Leithead², Shao-Meng Li^{4*}

4 ¹School of Metallurgy, Northeastern University, Shenyang, 110819, China

5 ²Air Quality Research Division, Environment and Climate Change Canada, Toronto, Ontario M3H 5T4,
6 Canada

7 ³Laboratory of Atmospheric Chemistry, Paul Scherrer Institute, Villigen 5232, Switzerland

8 ⁴State Key Joint Laboratory of Environmental Simulation and Pollution Control, College of Environmental
9 Sciences and Engineering, Peking University, Beijing, China 100871

10 **Correspondence:** Shao-Meng Li (shaomeng.li@pku.edu.cn)

11

12 **Short summary:** We presented yields and compositions of Si-containing SOA generated from the reaction
13 of cVMS (D3-D6) with OH radicals. NO_x played negative roles on cVMS SOA formation, while ammonium
14 sulfate seeds enhanced D3-D5 SOA yields at short photochemical ages under high-NO_x conditions. The
15 aerosol mass spectra confirmed that the components of cVMS SOA significantly relied on OH exposure. A
16 global cVMS-derived SOA source strength was estimated to understand SOA formation potentials of cVMS.

17

18 **Abstract**

19 Cyclic volatile methyl siloxanes (cVMS) are active ingredients in widely used consumer products, which
20 can volatilize into the atmosphere, thus attracting much attention due to their potential environmental risks.
21 While in the atmosphere the cVMS undergo oxidation yielding both gaseous and particulate products. The
22 aerosol yields and compositions from the OH oxidation of four cVMS (D3-D6) were determined under low

23 and high-NO_x conditions in an oxidation flow reactor. The aerosol yields progressively increased from D3
24 to D6, consistent with the volatilities and molecule weights of these cVMS. NO_x can restrict the formation
25 of SOA, leading to lower SOA yields under high-NO_x conditions than under low-NO_x conditions, with a
26 yield decrease between 0.05-0.30 depending on the cVMS. Ammonium sulfate seeds exhibited minor
27 impacts on SOA yields under low-NO_x conditions, but significantly increased the SOA yields in the oxidation
28 of D3-D5 at short photochemical ages under high-NO_x conditions. The mass spectra of the SOA showed a
29 dependence of its chemical compositions on OH exposure. At high exposures, equivalent to photochemical
30 ages of >6 days in the atmosphere, D4-D6 SOA mainly consisted of C_xH_y and C_xH_yO_zSi_n under low-NO_x
31 conditions, whereas they primarily contained N_mO_z, C_xH_y, C_xH_yO₁, C_xH_yO_{>1} and C_xH_yO_zSi_n under high-NO_x
32 conditions. Using the yield data from the present study and reported cVMS annual production, a global
33 cVMS-derived SOA source strength is estimated to be 0.16 Tg yr⁻¹, distributed over major urban centers.

34

35 **1 Introduction**

36 Secondary organic aerosols (SOA), which contribute 50-85% to the mass of atmospheric organic aerosols
37 (OA) (Glasius and Goldstein, 2016), are mainly formed via the partitioning of low volatility products from
38 oxidation of volatile organic compounds (VOCs), semi- and intermediate volatile organic
39 compounds(S/IVOCs) (Riipinen et al., 2012). SOA has attracted significant attention due to their important
40 impacts on climate, ecosystems and human health (Berndt et al., 2016). Global budgets of SOA remain an
41 unresolved issue despite extensive research, largely due to uncertainties associated with aerosol yields and
42 the presence of unconsidered SOA precursors.

43 As one type of anthropogenic VOC and potential SOA precursors, cyclic volatile methyl siloxanes (cVMS)
44 are widely used in industrial applications and personal care products (Genualdi et al., 2011; Krogseth et al.,

45 2013a). cVMS have been classified as high-volume chemicals with an annual production of millions of tons
46 globally (Rücker and Kümmerer, 2015; Ahrens et al., 2014). Studies of cVMS in the environment have
47 focused on investigating health and environmental impacts particularly due to their potential persistence,
48 bioaccumulation and toxicity (Guo et al., 2019; Liu et al., 2018; Farasani and Darbre, 2017; Xu et al., 2019;
49 Kim et al., 2018; Coggon et al., 2018). As a result, the European Council has proposed a restriction on the
50 octamethylcyclotetrasiloxane (D4) and decamethylcyclopentasiloxane (D5) content in wash-off personal
51 care products to a limit of 0.1 mass% by 2020 (Eur-Lex, 2018). The legislative actions notwithstanding,
52 knowledge of environmental behavior of cVMS **still needs to be further deepened** as compared to their
53 applications and economic significance (Rücker and Kümmerer, 2015).

54 It has been estimated that approximately 90% of cVMS are emitted into the atmosphere due to their high
55 saturation vapor pressures (Allen et al., 1997). Gas-phase cVMS have been observed in both indoor and
56 outdoor air. Tang et al. (2015) reported that cVMS accounted for about one third of total VOC mass
57 concentration in a classroom. Outdoor air concentrations of cVMS have also been measured at different sites
58 worldwide (Li et al., 2020; Wang et al., 2018; Rauert et al., 2018), increasing from rural to urban sites and
59 consistent with increasing population density (Rücker and Kümmerer, 2015). For example, at a rural site in
60 Sweden, the concentration of hexamethylcyclotrisiloxane (D3), D4, D5 and dodecamethylcyclohexasiloxane
61 (D6) were 0.94, 3.5, 13 and 1 ng/m³, respectively (Kierkegaard and Mclachlan, 2013), while they were 18,
62 55, 172 and 14 ng/m³ in urban areas of Toronto in Canada, respectively (Genualdi et al., 2011; Rauert et al.,
63 2018). cVMS have also been detected in the remote Arctic atmosphere, confirming their long-range transport
64 (Genualdi et al., 2011; Krogseth et al., 2013b). Atmospheric half-lives of cVMS are on the order of 30, 15,
65 10 and 6 days for D3-D6, respectively, which allow cVMS to exhibit a hemispherical distribution in the
66 atmosphere (Canada, 2008; Xiao et al., 2015). These lifetimes are driven mostly by reactions with the OH

67 radicals (Xiao et al., 2015; Wang et al., 2013), which generate silanols and dimeric products that can be
68 partitioned to condensed phases (Coggon et al., 2018; Sommerlade, 1993; Wu and Johnston, 2016). The loss
69 of cVMS in the atmosphere is slight through O₃ and NO₃ due to their small reaction rates, and by Cl atoms
70 on account of its low concentration **except for the spatial and temporal overlaps of cVMS emissions and Cl**
71 **sources.** (Atkinson, 1991; Alton and Browne, 2020).

72 It has been demonstrated that elemental Si is a frequent constituent of nanoparticles in rural and urban
73 areas (Phares et al., 2003; Rhoads, 2003; Bein, 2005; Bzdek et al., 2014) and in remote regions (Li and
74 Winchester, 1990; Li and Winchester, 1993). These Si-containing nanoparticles have previously been
75 attributed to ore smelting processes, but recent studies have shown that Si-containing species are one of the
76 main components in cVMS SOA, suggesting that the oxidation of cVMS may be an important source of Si
77 in atmospheric aerosols (Wu and Johnston, 2016, 2017). In a modeling study, the oxidation products of
78 cVMS (D4, D5 and D6) were considered to quantify the maximum potential for aerosol formation through
79 reactions with the OH radicals (Janecek et al., 2017). Chandramouli and Kamens (2001) demonstrated the
80 gas-particle partitioning of silanols from D5 oxidation by the OH radicals. Wu and Johnston (2016, 2017)
81 analyzed the chemical composition of secondary aerosols from OH oxidation of D4 and D5, showing a large
82 number of monomeric and dimeric products. Janecek et al. (2017, 2019) reported physical properties of
83 SOA generated by OH oxidation of D5, including hygroscopicity, cloud seeding potential and volatility.
84 Charan et al. (2022) measured SOA yields of D5 using chambers and flow tube reactors, **emphasizing the**
85 **importance of the relevant OH concentrations and exposures when extrapolating these laboratory results or**
86 **comparing with other studies.** These studies mainly focused on D5 and occasionally D4 but rarely others. To
87 better understand the SOA-forming potentials of typical cVMS in the atmosphere, accurate yields and
88 molecular compositions of SOA from the oxidation of cVMS under various atmospheric conditions are

89 needed.

90 In this work, the formation of SOA from the oxidation of four cVMS (D3-D6) by OH radical was
91 investigated in an oxidation flow reactor (OFR). Under various combinations of NO_x and ammonium sulfate
92 seed concentrations, the yields and compositions of SOA formed from the oxidation were measured using a
93 suite of instruments including a scanning mobility particle sizer (SMPS), a proton transfer reaction time of
94 flight mass spectrometer (PTR-ToF-MS) and an aerosol mass spectrometer (AMS). Based on these SOA
95 yields, the contribution of cVMS to SOA in the global atmosphere was estimated using reported cVMS
96 concentrations. The results obtained here can largely improve our understanding of the contribution and
97 composition of SOA from cVMS.

98 **2 Experiments and methods**

99 **2.1 Photo-oxidation experiments**

100 The reactions of cVMS with OH radicals were controlled at a constant temperature ($21\pm 1^\circ\text{C}$) and relative
101 humidity ($35\%\pm 2\%$) in a custom-made oxidation flow reactor (the Environment and Climate Change Canada
102 oxidation flow reactor, ECCC-OFR), which is shown in Fig. S1 of the Supplement and has been described
103 in detail previously (Li et al., 2019a). Briefly, the ECCC-OFR is a fused quartz cylinder (length: 50.8 cm,
104 inner diameter: 20.3 cm) equipped with a conical inlet and 7 outlets. Wall losses of particles and gases in the
105 ECCC-OFR have been shown to be lower than in other OFRs (Huang et al., 2017; Lambe et al., 2011;
106 Simonen et al., 2017; Li et al., 2019a). The length and full angle of cone inlet are 35.6 cm and 30° ,
107 respectively, designed to minimize the formation of jetting and recirculation in the OFR. The outlet at the
108 reactor center is a stainless-steel sampling port (inner diameter: 0.18 in) extending 12.7 cm long into the
109 ECCC-OFR. This sampling inlet reduces the impact of potential turbulent eddies caused by the back end of
110 the reactor. The remaining 6 outlets around the perimeter are designed to allow side flows to pass through

111 the OFR as a sheath flow, indirectly reducing wall losses of gases and particles inside the OFR upon sampling.
112 Ozone-free mercury UV lamps for generating OH radicals are housed in small quartz tubes around and in
113 parallel to the quartz reaction cylinder, and a large flow of air through each of these smaller quartz tubes is
114 used to remove the heat produced by the lamps. The relative humidity was adjusted by controlling the ratio
115 of dry air to wet air into the reactor, and was measured using a humidity sensor (Vaisala) at one of the sheath
116 flow outlets (side flows) of the reactor. The volume of the entire ECCC-OFR is about 16 L and the total flow
117 rate is 8 L min⁻¹, leading to a residence time of 2 min in the OFR.

118 OH radicals were produced through the reaction of water vapor with O(¹D) formed from O₃ photolysis at
119 254 nm. The OH concentration in the ECCC-OFR was regulated by controlling the input voltage and the
120 number of UV lamps. Methanol vapor, introduced into the ECCC-OFR through a bubbler containing
121 methanol solution, was used to determine the OH exposure (i.e., photochemical age) by tracking its decay
122 in the reactor from the reaction with the OH. The decay, or fractional loss, of gas-phase methanol,
123 [MeOH]/[MeOH]₀ was measured with the PTR-ToF-MS, and was used to calculate the OH concentration
124 via Equation 1,

$$125 \quad [\text{OH}] = -\frac{1}{k_{\text{MeOH}}} \ln \frac{[\text{MeOH}]}{[\text{MeOH}]_0} \quad (1)$$

126 where k_{MeOH} is the second-order rate constant of methanol reaction with OH at 298 K ($9.4 \times 10^{-13} \text{ cm}^3$
127 $\text{molecule}^{-1} \text{ s}^{-1}$). It was noted that the OH exposure measurement was offline, because methanol can affect the
128 OH reactivity with cVMS. Under low and high-NO_x conditions described below, the OH exposure varied in
129 the range of 5.5×10^{10} - 1.8×10^{12} and 8.2×10^{10} - 1.1×10^{12} molecules cm⁻³ s, respectively. They correspond
130 to 0.4-14.2 and 0.6-8.5 equivalent days (photochemical age), respectively, assuming that an average OH
131 concentration in air is 1.5×10^6 molecules cm⁻³ (Mao et al., 2009).

132 Pure D3-D6 cVMS compounds (solid D3 and liquid D4, D5 and D6) were placed in a glass U-type tube

133 and maintained at the room temperature. Vapors from these compounds (Table S1 of the Supplement) were
134 separately introduced into the ECCC-OFR by a small flow of zero air ($1-18 \text{ mL min}^{-1}$) passing over the
135 headspace of the U-tube containing the pure compounds. The concentrations of D3-D6 in the ECCC-OFR
136 ranged from 18 to 46 ppb (Table S2), depending on their volatilities. To study the influence of existing
137 particles on the SOA formation, ammonium sulfate (AS) seed particles were produced using an atomizer,
138 dried by a diffusion dryer and neutralized by a neutralizer and injected into the reactor without size selection.
139 The mass concentration of AS seed particles was approximately $30 \mu\text{g m}^{-3}$ for all experiments.

140 N_2O was used as a source of NO to achieve high- NO_x conditions (Lambe et al., 2017). NO_x conditions
141 were defined by the fate of peroxy radicals (RO_2), which was described by the reaction rate ratio (R_{NO}) of
142 $\text{RO}_2 + \text{NO}$ and $\text{RO}_2 + \text{HO}_2$ (Peng et al., 2017). The R_{NO} ratio increases with increasing OH exposures at a
143 constant concentration of N_2O (Li et al., 2019b). To achieve a constant branching ratio during the high- NO_x
144 experiments, the initial N_2O concentration in the OFR was varied (1.6%-8.0%) to maintain an R_{NO} value of
145 20 (Li et al., 2019b), as calculated using a model (OFR Exposures Estimator v3.1) (Peng et al., 2017). A
146 ratio of $R_{\text{NO}}=20$ indicates that 95% of RO_2 reacts with NO, ensuring the dominance of $\text{RO}_2 + \text{NO}$, which
147 represents conditions that are relevant for urban atmosphere (Peng et al., 2019). The role of $\text{RO}_2 + \text{RO}_2$ here
148 should be minor or negligible due to the low concentration of SOA precursors (cVMS, 18-46 ppb) (Lambe
149 et al., 2017; Peng et al., 2019; Li et al., 2019b). Peng et al. (2019) have reported that in the experiments
150 utilizing the injection of N_2O to achieve high- NO_x conditions, the relative importance of $\text{RO}_2 + \text{OH}$ was
151 generally negatively correlated with N_2O due to the suppressing effect of NO_x on OH radicals and the
152 increasing role of $\text{RO}_2 + \text{NO}$. Under low- NO_x conditions, N_2O was not introduced into the OFR, where the
153 RO_2 radicals dominantly interacted with HO_2 radicals, representing atmospheric scenarios with few NO_x
154 sources.

155 2.2 Characterization and analysis

156 The concentrations of cVMS in the OFR were measured online with PTR-ToF-MS (Ionicon Analytik
157 GmbH) (Liggio et al., 2016). The number and mass size distribution of aerosols was monitored using a
158 scanning mobility particle sizer (SMPS, TSI). The mass spectra and elemental composition of aerosols was
159 determined with a high-resolution time-of-flight aerosol mass spectrometer (HR-ToF-AMS, Aerodyne) and
160 analyzed with the AMS analysis software Squirrel (version 1.62G) and Pika (version 1.22G).

161 SOA mass yields (Y) were calculated via Equation 2,

$$162 \quad Y = \frac{\Delta C_{\text{SOA}}}{\Delta C_{\text{cVMS}}} \quad (2)$$

163 where ΔC_{SOA} and ΔC_{cVMS} are the mass concentrations of SOA formed and cVMS lost, respectively. The mass
164 concentration of SOA was determined by multiplying the effective aerosol density by the integrated SOA
165 volume concentration from the SMPS, subtracting the AS seed volume for experiments with AS seeds. The
166 effective aerosol density (ρ) was calculated for unseeded experiments through the following Equation 3
167 (Lambe et al., 2015),

$$168 \quad \rho = \frac{D_{va}}{D_m} \quad (3)$$

169 where D_{va} is the vacuum aerodynamic diameter obtained from the HR-ToF-AMS, and D_m is the electric
170 mobility diameter measured by the SMPS. The ρ varied in the range of 1.6-1.8 depending on the cVMS. The
171 same ρ value was also used in the seeded experiments. **It should be pointed out that the background values
172 in Table S3 have been subtracted when calculating the cVMS SOA yields.**

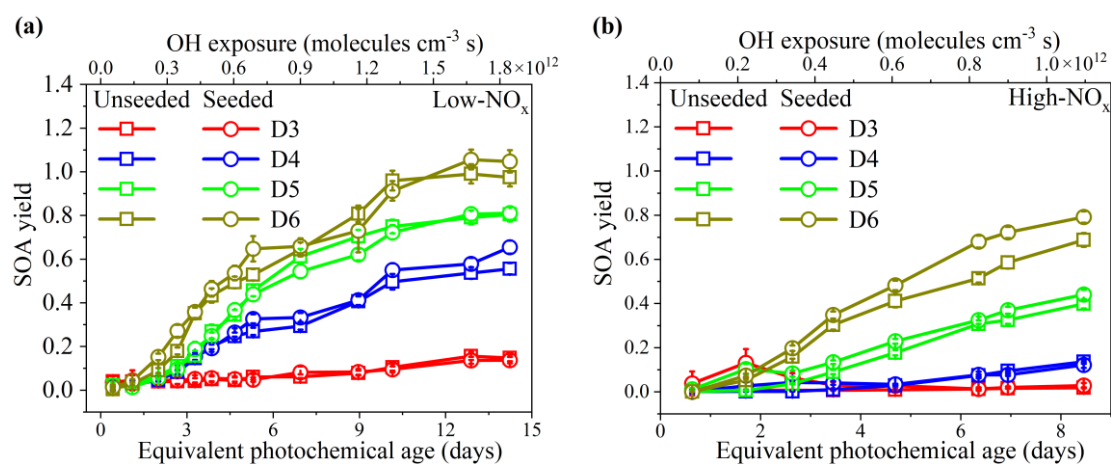
173 3 Results and discussion

174 3.1 SOA yields

175 **Taking the D5 SOA under low-NO_x and unseeded conditions as an example, the number and mass size
176 distributions of aerosols were shown in Fig. S2, which indicated that small particles dominated in the number,**

177 while large ones were prominent in mass. Compared to the size distributions of D5 SOA in low-NO_x
 178 experiments (Fig. S2a), the mode diameter of SOA increased for both number and mass size distribution
 179 under high-NO_x conditions (Fig. S2b), which suggests that larger particles are dominant in D5 SOA
 180 generated in high-NO_x experiments. The mass concentrations and time series of SOA measured by SMPS
 181 and AMS were shown in Table S4 and Fig. S3, respectively, which reflected a step-by-step pattern with
 182 increasing OH exposures.

183 Figure 1 shows the SOA yields from the photooxidation of the D3-D6 cVMS under low and high-NO_x
 184 conditions as a function of photochemical age (PA), i.e., time-integrated OH exposure, with and without AS
 185 seed particles. SOA yields have been widely used to estimate the potential of precursors to produce aerosol
 186 mass (Mcfiggans et al., 2019; Li et al., 2019a; Bruns et al., 2015; Lambe et al., 2015). As shown in Fig. 1,
 187 the cVMS SOA yields exhibited an overall increasing trend with PA, expressed in equivalent photochemical
 188 days, which agreed with the trend of D5 SOA yields reported by Janecek et al. (2019). Under low-NO_x
 189 conditions (Fig. 1a), SOA yields exhibited a slow growth, reaching a plateau after 10 equivalent days. This
 190 may be due to increased gas-phase fragmentation of cVMS to generate some higher volatility products,
 191 leading to a small increasing amplitude of partition ratio of species into SOA at longer photochemical ages.



192
 193 Figure 1. SOA yields from unseeded and seeded ($30 \mu\text{g m}^{-3}$) photooxidation of cVMS by OH radicals. **(a)**
 194 low-NO_x experiments; **(b)** high-NO_x experiments.

195 For the unseeded and low-NO_x experiments in Fig. 1a, SOA yields of four cVMS exhibited significant
196 differences in values over the same number of equivalent days. The SOA yields successively increased from
197 D3 to D6, consistent with the volatilities and molecular masses of the cVMS as well as their reaction rate
198 constants with the OH radical (Alton and Browne, 2020; Kim and Xu, 2017; Safron et al., 2015). The
199 maximum SOA yields of D3-D6 were (0.16±0.02), (0.56±0.03), (0.80±0.03) and (0.99±0.04), respectively,
200 occurring after a PA of 12 equivalent days. It has been reported that D5 SOA yields varied in the range of 0-
201 1.1 (Janecek et al., 2019; Wu and Johnston, 2017; Charan et al., 2022). Under a low OH exposure (~10¹⁰-
202 10¹¹ molecules cm⁻³ s), the D5 SOA yield (0.01-0.11) obtained here was similar to that (chamber, 0-0.057;
203 flow tube, 0.018-0.06) measured by Charan et al. (2022). However, under a high OH exposure of ~10¹¹-10¹²
204 molecules cm⁻³ s, the D5 SOA yield of 0.46-0.70 was higher than 0.22 and 0.14-0.35 (flow tube) reported
205 by Janecek et al. (2019) and Charan et al. (2022), respectively, which may be attributed to differences in
206 experimental conditions, such as differences in reactors, wall losses, SOA measurement methods,
207 determination of OH concentrations, and initial D5 concentrations (Table S5) (Janecek et al., 2019; Charan
208 et al., 2022). Although the amount of cVMS lost was variable, cVMS SOA yields positively depended on
209 SOA mass concentrations (Fig. S4), and this trend was observed in previous D5 SOA experiments with OH
210 oxidation (Wu and Johnston, 2017).

211 As shown in Fig. 1b, the order of SOA yields from the four cVMS under high-NO_x conditions was the
212 same as that under low-NO_x conditions. However, the SOA yields under high-NO_x conditions were generally
213 smaller than the corresponding yields at similar OH exposures under low-NO_x conditions, with a decrease
214 of 0.05-0.30 depending on the cVMS. Such a reduction suggests that NO_x can restrict the formation of cVMS
215 SOA. NO_x has been shown to reduce SOA yields for some anthropogenic alkanes (Li et al., 2019b), aromatics
216 (Ng et al., 2007a; Chan et al., 2009; Zhou et al., 2019), monoterpenes (Zhao et al., 2018) and other terpenes

217 (Ng et al., 2007b), attributable to the formation of higher volatility products (e.g., organic nitrates) generated
218 by $\text{RO}_2 + \text{NO}$ compared to $\text{RO}_2 + \text{HO}_2$ (Presto et al., 2005; Li et al., 2019b), which is also likely the case
219 here. The higher volatility products favor partitioning in the gas phase, thus reducing the potential for
220 forming SOA (Zhou et al., 2019). Moreover, high NO_x levels can suppress the formation of products for
221 nucleation, thereby reducing aerosol surface as a condensational sink and increasing the wall loss of
222 condensable species in an OFR under high- NO_x conditions (Zhao et al., 2018; Sarrafzadeh et al., 2016; Wildt
223 et al., 2014). Figure S5 indicates that the difference between SOA yields with and without NO_x decreased
224 with increasing silicon atoms within individual cVMS, indicating a less restricting effect of NO_x on the SOA
225 formation for larger cVMS. This means that high NO_x levels play a lesser role in the SOA yields of lower
226 volatility precursors.

227 SOA yields in the AS-seeded experiments under low and high- NO_x conditions are also shown in Figs. 1
228 and S5, indicating minimal impacts of the AS seed particles on SOA yields. A yield enhancement ratio
229 ($R_E = Y_{\text{seeded}}/Y_{\text{unseeded}}$, Fig. S6) was used to show the seed impacts more clearly. Under low- NO_x conditions,
230 the R_E values for all cVMS were close to 1.0 (Fig. S6a), suggesting negligible impact of AS seed particles
231 on SOA yields; however, under high- NO_x conditions, R_E was much larger (17.81, 13.18 and 15.51 for D3-
232 D5, respectively) at short PA but gradually decreased to 1.0 with increasing PA for D3-D5, while it was
233 always close to 1.0 for D6 regardless of PA (Fig. S6b). R_E values greater than 1.0 suggest that AS seed
234 particles played an enhancement role in the cVMS SOA formation, as similarly reported in SOA formation
235 from hydrocarbons (Sarrafzadeh et al., 2016; Lamkaddam et al., 2017; Li et al., 2019b). Under low- NO_x
236 conditions, the general lack of impact on cVMS SOA yields by the AS seed particles suggests that
237 condensation was not the main process driving SOA formation in cVMS oxidation. For the few cases of high
238 NO_x level at low PA, where R_E was >1 for D3-D5, it is possible that their early generations of oxidation

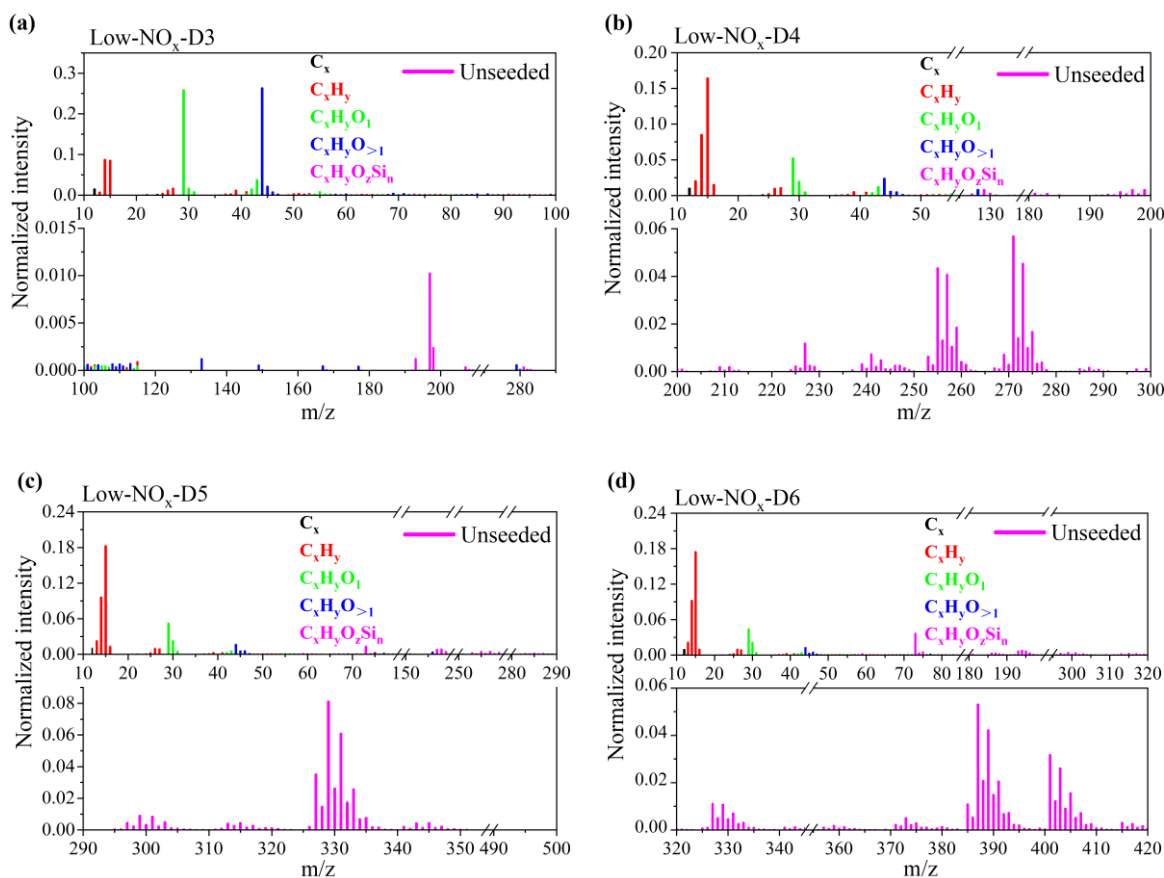
239 products were more volatile than successive generations of products and hence more prone to condensation
240 enhanced by AS seeds. As PA increased, further reactions of these early generation oxidation products with
241 OH radicals resulted in further generation products that were likely less volatile, thereby weakening the
242 enhancing role of AS seeds at high OH exposure. Such effect was less pronounced for D6, likely because its
243 oxidation products at different PA had similar volatilities. Figure S6b shows that the effect of AS seed
244 particles on SOA yields negatively correlated with the number of silicon atoms in the cVMS. Lower volatility
245 precursors (D5 and D6) may form lower volatile products, resulting in SOA yields less sensitive to the pre-
246 existing seeds. In fact, the oxidation products of D5 have been shown to be nearly non-volatile (Janecek et
247 al., 2019; Wu and Johnston, 2017).

248 **3.2 Aerosol compositions**

249 **3.2.1 Compositions of SOA under low-NO_x conditions.**

250 Figures 2 and S7 show the normalized HR-ToF-AMS mass spectra of cVMS SOA from unseeded
251 experiments under low-NO_x conditions at OH exposures of 9.0×10^{11} molecules cm⁻³ s. The mass spectral
252 signals can be identified as fragments with a formula of C_xH_yO_zSi_n. For D3 SOA, the most prominent peaks
253 were at m/z 44 and 29, dominated by CO₂⁺ and CHO⁺, which were tracers for organic acids (Ng et al., 2010),
254 alcohols and aldehydes (Lee et al., 2012), respectively. They may result from the oxidation of the methyl
255 groups in D3 by OH radicals. For the mass spectra of D4-D6 SOA, the two highest peaks at m/z 14 and 15
256 were CH₂⁺ and CH₃⁺, respectively. In addition, there were several dominant C_xH_yO_zSi_n peaks, which were
257 fragments of silicon-containing products. For the C_xH_yO_zSi_n group in D4 SOA, there were four typical peaks
258 at m/z 255, 257, 271 and 273, with formulae of C₄H₁₁O₇Si₃⁺, C₃H₉O₈Si₃⁺, C₃H₇O₉Si₃⁺ and C₃H₉O₉Si₃⁺,
259 respectively. The C_xH_yO_zSi_n fragment group containing Si of D5 SOA had three dominant peaks at m/z 327,
260 329 and 331, corresponding to C₁₂H₁₁O₂Si₅⁺, C₉H₉O₈Si₃⁺ and C₅H₁₅O₉Si₄⁺, respectively. For the C_xH_yO_zSi_n

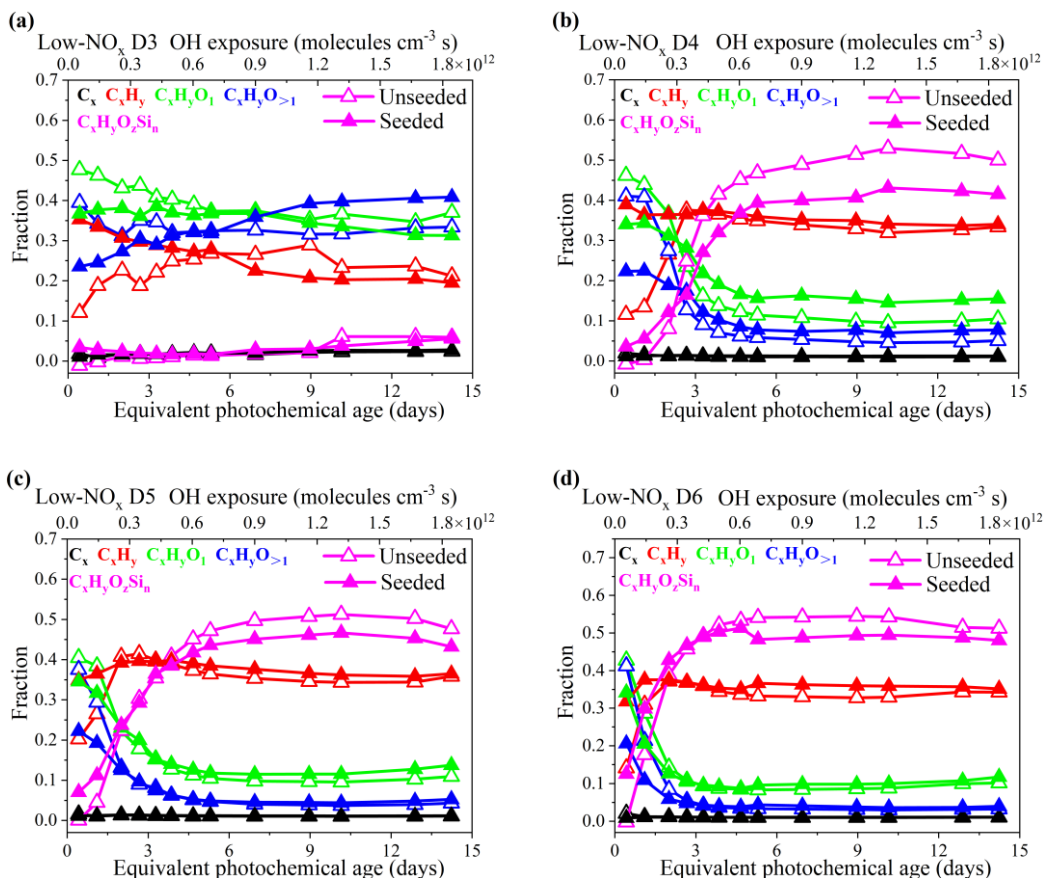
261 group containing Si in D6 SOA, there were five main peaks at m/z 73 (C_3H_9Si), 387 ($C_8H_{23}O_8Si_5^+$), 389
 262 ($C_8H_9O_9Si_5^+$), 401 ($C_9H_{21}O_{10}Si_4^+$) and 403 ($C_7H_{15}O_{12}Si_4^+$).



263
 264
 265 Figure 2. HR-ToF-AMS mass spectra of cVMS SOA at OH exposure of 9.0×10^{11} molecules cm^{-3} s under
 266 low- NO_x conditions in unseeded experiments. **a-d** represent the mass spectra of D3-D6 SOA, respectively.

267
 268 Figure 3 shows the evolution of different groups of ions in the HR-ToF-AMS spectra of the cVMS SOA
 269 as a function of PA in equivalent days. For D3-D6 under unseeded conditions, $C_xH_yO_1$ and $C_xH_yO_{>1}$ ions
 270 significantly decreased within 0-4 equivalent days of PA, but remained essentially unchanged when PA
 271 increased to 7-15 equivalent days. The C_xH_y ion increased to its peak value at about 9 equivalent days of PA
 272 for D3 and 2-3 equivalent days of PA for D4-D6, and then gradually decreased with further PA increases.
 273 The $C_xH_yO_zSi_n$ group of ions maintained an increasing trend until 9-10 days of PA, thereafter it decreased

274 slightly for D4-D6 SOA. The weighted values of the atomic number ratios Si/C (n/x) and Si/O (n/z) for the
275 $C_xH_yO_zSi_n$ groups in D5 and D6 SOA at different PA are plotted in Fig. S8, which can be used to indicate
276 the changes in the Si element of SOA. The Si/C ratio at initial SOA formation stage was close to that (0.50)
277 in D5 and D6 molecules, and then increased continuously with increasing PA. The Si/O ratio kept increasing
278 from 0.53 to 1.15 for D5 SOA and from 0.72 to 1.32 for D6 SOA, but varying around 1.0 that was the Si/O
279 ratio in D5 and D6. While it is difficult to separate the effect of fragmentation due to the AMS ionization
280 process, the relative changes of group intensities and the evolution of Si/C and Si/O in $C_xH_yO_zSi_n$ over
281 different PA may be attributed to the evolution of cVMS when oxidized by the OH radicals. The initial step
282 of OH radicals oxidation can be considered as OH abstracting a H atom from the methyl groups on the -Si-
283 O- ring of the cVMS to form Si-containing radicals, which may generate OH and CH₂OH substitution
284 products, such as silanol and silyl methanol (Wu and Johnston, 2016; Alton and Browne, 2020). Such Si-
285 containing products may partition into SOA and result in an appearance of $C_xH_yO_zSi_n$ ions in the AMS mass
286 spectra, thereby decreasing the initial ratio of Si/O (D5: 0.53; D6: 0.72). Notably, one previous study reported
287 that one of oxidation products of D5, 1-hydroxynonamethylcyclopentasiloxane (D₄TOH), has been detected
288 in ambient particulate matter (Milani et al., 2021). As the reaction progresses, the Si-O bonds may be cleaved
289 from OH radical attack, which may reduce the number of O atoms, leading to an increase of Si/O with PA.
290 The continued breaking of Si-O bonds would lead to fragmentation and more volatile products, which caused
291 lower SOA yield and $C_xH_yO_zSi_n$ fraction at longer PA (Figs. 1 and 3).



292

293

294 Figure 3. Fraction of C_x, C_xH_y, C_xH_yO₁, C_xH_yO_{>1} and C_xH_yO_zSi_n ion groups for SOA derived from the
 295 oxidation of cVMS (a-d) by OH radicals at different photochemical ages under low-NO_x conditions.

296 Empty and solid triangles represent experimental data under unseeded and seeded conditions, respectively.

297

298 As shown in Fig. 3, the presence of seeds led to some changes in the evolution trends of ion groups in the
 299 AMS spectra. For instance, the initial fraction of C_xH_y in seeded experiments was larger than that in unseeded
 300 experiments, which may be related to the volatility of species containing C_xH_y that may be more easily
 301 deposited in the presence of seeds, whereas C_xH_yO₁ and C_xH_yO_{>1} exhibited opposite changes. The presence
 302 of seeds led to larger initial and smaller steady-state C_xH_yO_zSi_n fractions than those in unseeded experiments.
 303 Regardless of the presence of seeds, C_xH_y, C_xH_yO₁ and C_xH_yO_{>1} mainly contributed to the composition of
 304 all cVMS SOA at initial OH radicals oxidation, but D4-D6 SOA primarily consisted of C_xH_y and C_xH_yO_zSi_n

305 after 6 equivalent days.

306 **3.2.2 Compositions of SOA under high-NO_x conditions.**

307 Figure S9 shows the HR-ToF-AMS mass spectra of cVMS SOA from unseeded experiments under high-
308 NO_x conditions at OH exposures of 9.0×10^{11} molecules cm⁻³ s (~6.9 d). Compared to that under low-NO_x
309 conditions (Figs. 2 and S7), there was one additional N-containing group (N_mO_z) in the SOA mass spectra
310 under high-NO_x conditions, which accounted for 16%-31%. For the mass spectra of D3-D6 SOA originating
311 from unseeded experiments under high-NO_x conditions in Fig. S9, the dominating peaks of the N_mO_z family
312 were m/z 30 (NO⁺) and m/z 46 (NO₂⁺). The common main peaks were located at m/z 30 (NO⁺) for cVMS
313 SOA, m/z 44 (CO₂⁺) for D3-D4 SOA, and m/z 46 (NO₂⁺) for D4-D6 SOA. In addition, there were other
314 primary peaks at m/z 29 (CHO⁺) for D4 SOA, while m/z 15 (CH₃⁺) and m/z 28 (CO⁺) for D5-D6 SOA. The
315 m/z 28 (CO⁺), similar with m/z 44 (CO₂⁺), is considered as a tracer for organic acids (Ng et al., 2010). In the
316 mass spectra for D3-D6 SOA under high-NO_x conditions, the presence of NO⁺ (m/z 30) and NO₂⁺ (m/z 46)
317 illustrated the formation of nitrates in SOA (Ng et al., 2007b).

318 For the C_xH_yO_zSi_n group in the D4 SOA mass spectrum under high-NO_x conditions, the dominating peaks
319 and their formulas were same as those under low-NO_x conditions. For the C_xH_yO_zSi_n group in D5 SOA, in
320 addition to two typical peaks at m/z 327 and 329 in the low-NO_x experiments, there was another prominent
321 peak at m/z 328, with a formula C₈H₁₂O₅Si₅. The C_xH_yO_zSi_n group in D6 SOA had three typical peaks at m/z
322 73 (C₃H₉Si), m/z 387 (C₈H₂₃O₈Si₅⁺) and m/z 401 (C₉H₂₁O₁₀Si₄⁺). For the C_xH_yO_zSi_n groups in cVMS SOA,
323 there was little difference in the x, y, z and n value assignment of C_xH_yO_zSi_n peaks in SOA generated under
324 low-NO_x and high-NO_x conditions, suggesting the formation of similar Si-containing oxidation products.

325 For cVMS SOA under high-NO_x conditions, the evolution of family groups as a function of OH exposure
326 was summarized in Fig. S10. The dominated composition at initial stage was C_xH_yO_{>1} groups for D3-D6

327 SOA. At equivalent days larger than 6, D3 SOA primarily consisted of $C_xH_yO_{>1}$, N_mO_z and $C_xH_yO_1$ groups,
328 while D4-D6 SOA was mainly composed of $C_xH_yO_zSi_n$, N_mO_z , $C_xH_yO_1$, C_xH_y and $C_xH_yO_{>1}$ groups. Figure
329 S10 also shows influences of seeds on the evolution of family groups under high- NO_x conditions. It was
330 observed that all groups in D3-D6 SOA displayed similar change trends regardless of the existence of seeds.
331 As shown in Fig. S11, the trend of the weighted values of the atomic ratio Si/O in the $C_xH_yO_zSi_n$ groups at
332 different photochemical ages under high- NO_x conditions was similar to that in low- NO_x experiments.
333 However, the Si/C ratios remained almost unchanged, and were close to the initial value (0.5) in cVMS. This
334 may be attributed to possible suppression of cleavage of methyl groups from the -Si-O- ring of the cVMS
335 under high- NO_x conditions.

336 **4 Conclusions and implications**

337 The yields and compositions of SOA generated from the photooxidation of four cVMS (D3-D6) with OH
338 radicals were investigated using an oxidation flow reactor. cVMS SOA yields exhibited an overall increasing
339 trend with PA, and their values gradually increased with cVMS from D3 to D6. SOA formations depended
340 on NO_x , as shown by smaller SOA yields under high- NO_x conditions. Ammonium sulfate seeds significantly
341 enhanced SOA yields of D3-D5 at short PA under high- NO_x conditions. The SOA mass spectra showed that
342 Si-containing species were one of main chemical compositions at PA of >6 days.

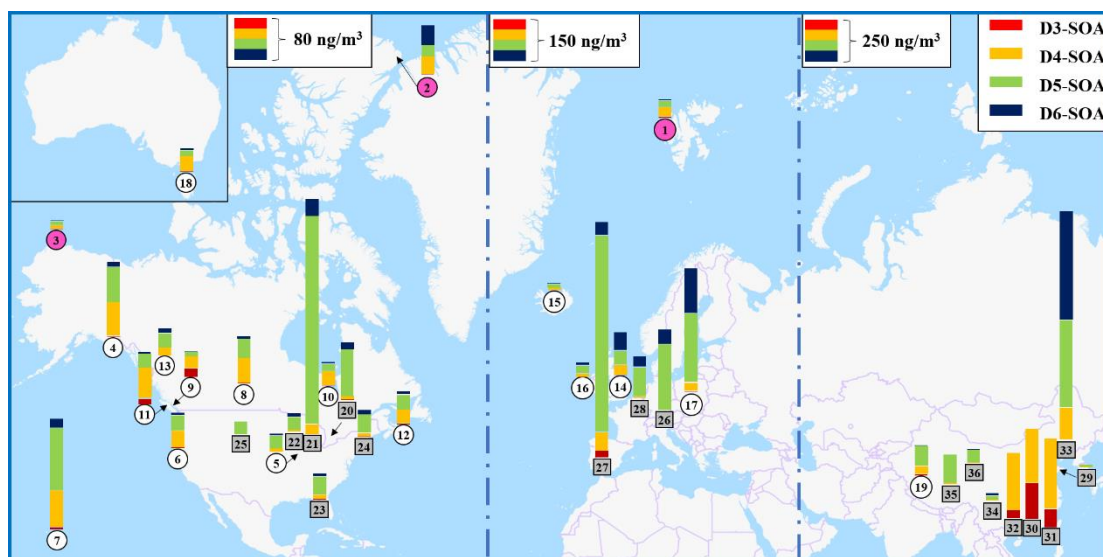
343 To evaluate the potential contributions of cVMS to SOA formation in the atmosphere, global SOA
344 concentrations produced from cVMS were estimated according to the cVMS SOA yields measured in this
345 work and using the cVMS concentrations reported from multiple studies, which were listed in Table S6.
346 Here, the high- NO_x SOA yields under the seeded conditions at 8.5 equivalent days (D3: 0.028; D4: 0.122;
347 D5: 0.441; D6: 0.792) are employed in the calculation of cVMS SOA concentrations at urban sites, while
348 the low- NO_x SOA yields under the unseeded conditions at 14.2 equivalent days (D3: 0.148; D4: 0.556; D5:

0.805; D6: 0.975) are used to estimate cVMS SOA at background and polar sites. The selected equivalent days were within the atmospheric half-lives (6-30 days) of cVMS. Figure 4 shows the global concentration distribution of SOA from four cVMS (D3-D6) at 36 sites worldwide estimated by the Equation 4,

$$C_{\text{cVMS-SOA}} = C_{\text{cVMS}} \times \frac{\Delta C_{\text{cVMS}}}{C_{\text{in-cVMS}}} \times Y \quad (4)$$

where C_{cVMS} and $C_{\text{cVMS-SOA}}$ are the mass concentration of cVMS reported from literatures and cVMS SOA estimated in global sites, respectively; $C_{\text{in-cVMS}}$ and ΔC_{cVMS} are the mass concentration of initial and lost cVMS at the selected equivalent days during the experiments of this work, respectively (Table S7); Y is the cVMS SOA mass yields mentioned above. It was noted that the estimations from the Equation 4 were based on assumptions that the lost cVMS ratio is not affected by the cVMS concentration and the background $C_{\text{cVMS-SOA}}$ is zero. Although there may be some uncertainties in extrapolating our results to the real atmosphere, such as larger cVMS concentrations and SOA yields, our extrapolations may provide an upper limit for evaluating cVMS SOA. Table S6 summarizes the details regarding sites and concentrations of cVMS SOA. The derived concentrations of cVMS SOA varies significantly among urban, background and polar sites. The total cVMS SOA concentrations in urban areas are the highest, up to 1324 ng/m³. They are 18.9-428 and 13.8-138.8 ng/m³ for background and Arctic sites, respectively. cVMS SOA concentrations in urban regions of Asia (sites 29-36) and Europe (sites 26-28) are generally larger than that of North America (sites 20-25). In China, the total cVMS SOA concentrations in urban sites range from 15.5 to 1324 ng/m³. The main precursors of cVMS SOA are different among Chinese cities. For three cities along the southeast coast of China (Guangzhou, Macau and Foshan), the dominant precursors of cVMS SOA are D3 and D4, which are related to industrial emissions of these two siloxanes in this region (Wang et al., 2001). For Dalian in China, mainly D5 and D6 contribute to cVMS SOA, which have the highest concentrations among all sites. This can be attributed to the industrial production of D5 and D6 and the use of personal care products

371 in Dalian (Li et al., 2020). In the other Chinese urban areas with reported cVMS concentrations (Lhasa,
 372 Golmud, Kunming and Yantai), the total cVMS SOA concentrations are considerably smaller than those in
 373 the urban areas above, with D5 acting as the main precursor, which may be ascribed to the relatively low
 374 population densities in these cities (Wang et al., 2018).



375
 376 Figure 4. Global concentrations of cVMS SOA (ng/m³) on the basis of the cVMS concentrations
 377 reported from multiple studies and the cVMS SOA yields measured in this work. The numbers of polar,
 378 background and urban sites are enclosed in pink, white circles and gray boxes, respectively. The details
 379 about cVMS and SOA concentrations at different sites were summarized in Table S6 of the Supplement.

380
 381 At urban sites in Europe and North America, cVMS SOA concentrations are reported in the range of 138-
 382 813 ng/m³ and 22.9-437 ng/m³, respectively. Among these cVMS, D5 is the main contributor to cVMS SOA
 383 at these locations, averaging 80.1% of total cVMS SOA. This contribution is higher than that (73.6%) at
 384 Chinese urban sites. For instance, D5 SOA is calculated to be 684 ng/m³ in Catalan, Spain, 387 ng/m³ in
 385 Chicago, USA, 229 ng/m³ in Zurich, Switzerland and 99 ng/m³ in Paris, France, where there are high levels
 386 of economic activities and high population densities. These results suggest that personal care products as a

387 main source of D5 may be the most important anthropogenic origins of Si-containing SOA in Europe and
388 North America. It was noted that the D5 SOA concentration (13.38-683.57 ng/m³) estimated here is far more
389 than that (0.016-0.206 ng/m³) reported by Milani et al. (2021), who obtained their data using semi-quantified
390 concentrations of D₄TOH (first-generation D5 SOA product) extracted from PM_{2.5} samples in Atlanta and
391 Houston. The difference may be mainly attributed to the missing analysis of multi-generation SOA products
392 or dimers (Wu and Johnston, 2016, 2017). Pennington et al. (2021) utilized the developed CMAQ model
393 to investigate the concentration of D5 SOA in the urban area of Los Angeles, and the model data (21 ng/m³)
394 was within these values here.

395 At background and Arctic sites, cVMS SOA are primarily derived from D4 and D5. The background sites
396 are located in mountains, rural areas, forested areas, lakes and at high altitudes. The three highest cVMS
397 SOA concentrations at background sites are located at Kosetice in the Czech Republic (428 ng/m³), Hilo,
398 Hawaii, USA (203 ng/m³) and Tibetan Plateau in China (174 ng/m³), where the contribution percentages of
399 SOA from both D4 and D5 are 62.6%, 90.3% and 93.4%, respectively. The cVMS SOA concentrations at
400 the Little Fox Lake site in Yukon, Canada is the highest (138.8 ng/m³) among the four locations in the Arctic,
401 91% of which is accounted for by both D4 and D5 SOA. The dominance of D4 and D5 SOA in both
402 background and the Arctic regions highlights their persistence in atmosphere and the potential for long-range
403 atmospheric transport.

404 Furthermore, global concentration distribution of Si-containing SOA estimated for the four cVMS (D3-
405 D6) at 36 sites worldwide is also presented in Table S6, which clearly shows the global importance of Si in
406 SOA with the estimated percentages of cVMS SOA that contains the Si element. For example, up to 49.2%
407 and 31.2% of cVMS SOA contained Si elements in background and urban sites, respectively. These results
408 are similar to the summary observations that reported percentages of aerosols with a Si mole fraction >0.01

409 (%) at different sites (Bzdek et al., 2014). The above results demonstrated that Si is a frequent component of
410 SOA in background and urban areas.

411 The global annual production of D4, D5 and D6 is about 1, 0.1 and 0.01 Tg·yr⁻¹, respectively, and 90% of
412 these cVMS is eventually released into the atmosphere (Li et al., 2020; Genualdi et al., 2011; Wang et al.,
413 2013; Sakurai et al., 2019). Based on the results shown in Fig. 4, the annual production of cVMS (D4-D6)
414 SOA was estimated to be 0.16 Tg·yr⁻¹, which was about 5.5% of SOA (2.9 Tg·yr⁻¹) produced from mobile
415 source emissions in the USA and 5-8 times of SOA generated by Athabasca oil sands (0.02-0.03 Tg·yr⁻¹, one
416 of the largest sources of anthropogenic secondary organic aerosols in North America) (Tkacik et al., 2014;
417 Liggio et al., 2016). Moreover, it was also 0.8% and 2.3% of isoprene-SOA (20 Tg·yr⁻¹) and monoterpenes-
418 SOA (7 Tg·yr⁻¹) (typical biogenic SOA), respectively, indicating the potential importance of cVMS SOA
419 (Jokinen et al., 2015). While these cVMS SOA sources may seem small, they can make substantially higher
420 contributions to ambient air SOAs in population centers where cVMS compounds are primarily used.

421

422 **Author contributions**

423 CH designed and conducted all experiments; CH and HY analyzed the data and prepared the paper with
424 contributions from KL, PL, JL, AL and SML. SML supervised the project.

425

426 **Competing interests**

427 The authors declare that they have no conflict of interest.

428 **Acknowledgements**

429 This project was supported by Environment and Climate Change Canada's Climate and Clean Air Program
430 (CCAP); the National Natural Science Foundation of China (42077198); the LiaoNing Revitalization Talents

431 Program (XLYC1907185); the Fundamental Research Funds for the Central Universities (N2025011).

432

433 **References**

434 Ahrens, L., Harner, T., and Shoeib, M.: Temporal Variations of Cyclic and Linear Volatile Methylsiloxanes in the
435 Atmosphere Using Passive Samplers and High-Volume Air Samplers, *Environ. Sci. Technol.*, 48, 9374-9381,
436 <https://doi.org/10.1021/es502081j>, 2014.

437 Allen, R., Kochs, P., and Chandra, G.: Industrial Organosilicon Materials, Their Environmental Entry and
438 Predicted Fate, *Springer*, 3, 1-25, https://doi.org/10.1007/978-3-540-68331-5_1, 1997.

439 Alton, M. and Browne, E.: Atmospheric Chemistry of Volatile Methyl Siloxanes: Kinetics and Products of
440 Oxidation by OH Radicals and Cl Atoms, *Environ. Sci. Technol.*, 54, 5992-5999,
441 <https://dx.doi.org/10.1021/acs.est.0c01368>, 2020.

442 Atkinson, R.: Kinetics of the Gas-Phase Reactions of a Series of Organosilicon Compounds with OH and NO₃
443 Radicals and O₃ at 297 ± 2 K, *Environ. Sci. Technol.*, 25, 863-866, <https://doi.org/10.1021/es00017a005>, 1991.

444 Bein, K., Zhao, Y., Wexler, A., Johnston, M.: Speciation of Size-Resolved Individual Ultrafine Particles in
445 Pittsburgh, Pennsylvania, *J. Geophys. Res.*, 110, D07S05, <https://doi.org/10.1029/2004jd004708>, 2005.

446 Berndt, T., Richters, S., Jokinen, T., Hyttinen, N., Kurtén, T., Otkjaer, R., Kjaergaard, H., Stratmann, F., Herrmann,
447 H., Sipilä, M., Kulmala, M., and Ehn, M.: Hydroxyl Radical-Induced Formation of Highly Oxidized Organic
448 Compounds, *Nat. Commun.*, 7, 1-8, <https://doi.org/10.1038/ncomms13677>, 2016.

449 Bruns, E., Haddad, I., Keller, A., Klein, F., Kumar, N., Pieber, S., Corbin, J., Slowik, J., Brune, W., Baltensperger,
450 U., and Prévôt, A.: Inter-Comparison of Laboratory Smog Chamber and Flow Reactor Systems on Organic
451 Aerosol Yield and Composition, *Atmos. Meas. Tech.*, 8, 2315-2332, <https://doi.org/10.5194/amt-8-2315-2015>,
452 2015.

453 Bzdek, B., Horan, A., Pennington, M., Janecek, N., Baek, J., Stanier, C., and Johnston, M.: Silicon is a Frequent
454 Component of Atmospheric Nanoparticles, *Environ. Sci. Technol.*, 48, 11137-11145,
455 <https://doi.org/10.1021/es5026933>, 2014.

456 Canada, E. C. a. H.: [https://www.ec.gc.ca/ese-ees/FC0D11E7-DB34-41AA-B1B3-E66EFD8813F1/batch2_540-](https://www.ec.gc.ca/ese-ees/FC0D11E7-DB34-41AA-B1B3-E66EFD8813F1/batch2_540-97-6_en.pdf)
457 [97-6_en.pdf](https://www.ec.gc.ca/ese-ees/FC0D11E7-DB34-41AA-B1B3-E66EFD8813F1/batch2_540-97-6_en.pdf) last access: 9 February 2022, 2008.

458 Chan, A., Kautzman, K., Chhabra, P., Surratt, J., Chan, M., Crouse, J., Kürten, A., Wennberg, P., Flagan, R., and
459 Seinfeld, J.: Secondary Organic Aerosol Formation from Photooxidation of Naphthalene and Alkyl naphthalenes:

460 Implications for Oxidation of Intermediate Volatility Organic Compounds (IVOCs), *Atmos. Chem. Phys.*, 9,
461 3049–3060, <https://doi.org/10.5194/acp-9-3049-2009>, 2009.

462 Chandramouli, B., Kamens, R.: The Photochemical Formation and Gas-Particle Partitioning of Oxidation
463 Products of Decamethyl Cyclopentasiloxane and Decamethyl Tetrasiloxane in the Atmosphere, *Atmos.*
464 *Environ.*, 35, 87-95, [https://doi.org/10.1016/S1352-2310\(00\)00289-2](https://doi.org/10.1016/S1352-2310(00)00289-2), 2001.

465 Charan, S., Huang, Y., Buenconsejo, R., Li, Q., Cocker III, D., and Seinfeld, J.: Secondary Organic Aerosol
466 Formation from the Oxidation of Decamethylcyclopentasiloxane at Atmospherically Relevant OH
467 Concentrations, *Atmos. Chem. Phys.*, 22, 917-928, <https://doi.org/10.5194/acp-22-917-2022>, 2022.

468 Coggon, M., McDonald, B., Vlasenko, A., Veres, P., Bernard, F., Koss, A., Yuan, B., Gilman, J., Peischl, J., Aikin,
469 K., DuRant, J., Warneke, C., Li, S.-M., and Gouw, J.: Diurnal Variability and Emission Pattern of
470 Decamethylcyclopentasiloxane (D5) from the Application of Personal Care Products in Two North American
471 Cities, *Environ. Sci. Technol.*, 52, 5610-5618, <https://doi.org/10.1021/acs.est.8b00506>, 2018.

472 EUR-Lex: [https://eur-lex.europa.eu/legal-](https://eur-lex.europa.eu/legal-content/EN/TXT/?uri=uriserv:OJ.L_.2018.006.01.0045.01.ENG&toc=OJ:L:2018:006:TOCECHA)
473 [content/EN/TXT/?uri=uriserv:OJ.L_.2018.006.01.0045.01.ENG&toc=OJ:L:2018:006:TOCECHA](https://eur-lex.europa.eu/legal-content/EN/TXT/?uri=uriserv:OJ.L_.2018.006.01.0045.01.ENG&toc=OJ:L:2018:006:TOCECHA), last
474 access: 25 November 2021, 2018.

475 Farasani, A. and Darbre, P.: Exposure to Cyclic Volatile Methylsiloxanes (cVMS) Causes Anchorage-Independent
476 Growth and Reduction of BRCA1 in Non-Transformed Human Breast Epithelial Cells, *J. Appl. Toxicol.*, 37,
477 454-461, <https://doi.org/10.1002/jat.3378>, 2017.

478 Genualdi, S., Harner, T., Cheng, Y., Macleod, M., Hansen, K., Egmond, R., Shoeib, M., and Lee, S.: Global
479 Distribution of Linear and Cyclic Volatile Methyl Siloxanes in Air, *Environ. Sci. Technol.*, 45, 3349-3354,
480 <https://doi.org/10.1021/es200301j>, 2011.

481 Glasius, M. and Goldstein, A.: Recent Discoveries and Future Challenges in Atmospheric Organic Chemistry,
482 *Environ. Sci. Technol.*, 50, 2754-2764, <https://doi.org/10.1021/acs.est.5b05105>, 2016.

483 Guo, J., Zhou, Y., Cui, J., Zhang, B., and Zhang, J.: Assessment of Volatile Methylsiloxanes in Environmental
484 Matrices and Human Plasma, *Sci. Total. Environ.*, 668, 1175-1182,
485 <https://doi.org/10.1016/j.scitotenv.2019.03.092>, 2019.

486 Huang, Y., Coggon, M., Zhao, R., Lignell, H., Bauer, M., Flagan, R., and Seinfeld, J.: The Caltech Photooxidation
487 Flow Tube reactor: Design, Fluid Dynamics and Characterization, *Atmos. Meas. Tech.*, 10, 839-867,
488 <https://doi.org/10.5194/amt-10-839-2017>, 2017.

489 Janeček, N., Hansen, K., and Stanier, C.: Comprehensive Atmospheric Modeling of Reactive Cyclic Siloxanes

490 and their Oxidation Products, *Atmos. Chem. Phys.*, 17, 8357-8370, <https://doi.org/10.5194/acp-17-8357-2017>,
491 2017.

492 Janecek, N., Marek, R., Bryngelson, N., Singh, A., Bullard, R., Brune, W., and Stanier, C.: Physical Properties
493 of Secondary Photochemical Aerosol from OH Oxidation of a Cyclic Siloxane, *Atmos. Chem. Phys.*, 19, 1649-
494 1664, <https://doi.org/10.5194/acp-19-1649-2019>, 2019.

495 Jokinen, T., Berndt, T., Makkonen, R., Kerminen, V., Junninen, H., Paasonen, P., Stratmann, F., Herrmann, H.,
496 Guenther, A., Worsnop, D., Kulmala, M., Ehn, M., and Sipilä, M.: Production of Extremely Low Volatile
497 Organic Compounds from Biogenic Emissions: Measured Yields and Atmospheric Implications, *Proc. Natl.*
498 *Acad. Sci. U S A.*, 112, 7123-7128, <https://doi.org/10.1073/pnas.1423977112>, 2015.

499 Kierkegaard, A. and McLachlan, M.: Determination of Linear and Cyclic Volatile Methylsiloxanes in Air at a
500 Regional Background Site in Sweden, *Atmos. Environ.*, 80, 322-329,
501 <https://doi.org/10.1016/j.atmosenv.2013.08.001>, 2013.

502 Kim, J. and Xu, S.: Quantitative Structure-Reactivity Relationships of Hydroxyl Radical Rate Constants for Linear
503 and Cyclic Volatile Methylsiloxanes, *Environ. Toxicol. Chem.*, 36, 3240-3245, <https://doi.org/10.1002/etc.3914>,
504 2017.

505 Kim, J., Mackay, D., and Whelan, M.: Predicted Persistence and Response Times of Linear and Cyclic Volatile
506 Methylsiloxanes in Global and Local Environments, *Chemosphere*, 195, 325-335,
507 <https://doi.org/10.1016/j.chemosphere.2017.12.071>, 2018.

508 Krogseth, I., Zhang, X., Lei, Y., Wania, F., and Breivik, K.: Calibration and Application of a Passive Air Sampler
509 (XAD-PAS) for Volatile Methyl Siloxanes, *Environ. Sci. Technol.*, 47, 4463-4470,
510 <https://doi.org/10.1021/es400427h>, 2013a.

511 Krogseth, I., Kierkegaard, A., McLachlan, M., Breivik, K., Hansen, K., and Schlabach, M.: Occurrence and
512 Seasonality of Cyclic Volatile Methyl Siloxanes in Arctic Air, *Environ. Sci. Technol.*, 47, 502-509,
513 <https://doi.org/10.1021/es3040208>, 2013b.

514 Lambe, A., Chhabra, P., Onasch, T., Brune, W., Hunter, J., Kroll, J., Cummings, M., Brogan, J., Parmar, Y.,
515 Worsnop, D., Kolb, C., and Davidovits, P.: Effect of Oxidant Concentration, Exposure Time, and Seed Particles
516 on Secondary Organic Aerosol Chemical Composition and Yield, *Atmos. Chem. Phys.*, 15, 3063-3075,
517 <https://doi.org/10.5194/acp-15-3063-2015>, 2015.

518 Lambe, A., Ahern, A., Williams, L., Slowik, J., Wong, J., Abbatt, J., Brune, W., Ng, N., Wright, J., Croasdale, D.,
519 Worsnop, D., Davidovits, P., and Onasch, T.: Characterization of Aerosol Photooxidation Flow Reactors:

520 Heterogeneous Oxidation, Secondary Organic Aerosol Formation and Cloud Condensation Nuclei Activity
521 Measurements, *Atmos. Meas. Tech.*, 4, 445-461, <https://doi.org/10.5194/amt-4-445-2011>, 2011.

522 Lambe, A., Massoli, P., Zhang, X., Canagaratna, M., Nowak, J., Daube, C., Yan, C., Nie, W., Onasch, T., Jayne,
523 J., Kolb, C., Davidovits, P., Worsnop, D., and Brune, W.: Controlled Nitric Oxide Production via $O(^1D) + N_2O$
524 Reactions for Use in Oxidation Flow Reactor Studies, *Atmos. Meas. Tech.*, 10, 2283-2298,
525 <https://doi.org/10.5194/amt-10-2283-2017>, 2017.

526 Lamkaddam, H., Gratien, A., Pangu, E., Cazaunau, M., Varrault, B., and Doussin, J.: High-NO_x Photooxidation
527 of n-Dodecane: Temperature Dependence of SOA Formation, *Environ Sci Technol*, 51, 192-201,
528 <https://doi.org/10.1021/acs.est.6b03821>, 2017.

529 Lee, A., Hayden, K., Herckes, P., Leaitch, W., Liggio, J., Macdonald, A., and Abbatt, J.: Characterization of
530 Aerosol and Cloud Water at a Mountain Site During WACS 2010: Secondary Organic Aerosol Formation
531 through Oxidative Cloud Processing, *Atmos. Chem. Phys.*, 12, 7103-7116, [https://doi.org/10.5194/acp-12-](https://doi.org/10.5194/acp-12-7103-2012)
532 [7103-2012](https://doi.org/10.5194/acp-12-7103-2012), 2012.

533 Li, K., Liggio, J., Lee, P., Han, C., Liu, Q., and Li, S.-M.: Secondary Organic Aerosol Formation from α -Pinene,
534 Alkanes, and Oil Sand-Related Precursors in a New Oxidation Flow Reactor, *Atmos. Chem. Phys.*, 19, 9715-
535 9731, <https://doi.org/10.5194/acp-19-9715-2019>, 2019a.

536 Li, K., Liggio, J., Han, C., Liu, Q., Moussa, S., Lee, P., and Li, S.-M.: Understanding the Impact of High-NO_x
537 Conditions on the Formation of Secondary Organic Aerosol in the Photooxidation of Oil Sand-Related
538 Precursors, *Environ. Sci. Technol.*, 53, 14420-14429, <https://doi.org/10.1021/acs.est.9b05404>, 2019b.

539 Li, Q., Lan, Y., Liu, Z., Wang, X., Wang, X., Hu, J., and Geng, H.: Cyclic Volatile Methylsiloxanes (cVMSs) in
540 the Air of the Wastewater Treatment Plants in Dalian, China-Levels, Emissions, and Trends, *Chemosphere*, 256,
541 1-8, <https://doi.org/10.1016/j.chemosphere.2020.127064>, 2020.

542 Li, S.-M. and Winchester, J.: Particle Size Distribution and Chemistry of Late Winter Arctic Aerosols, *J. Geophys.*
543 *Res.*, 95, 13897-13908, <https://doi.org/10.1029/J095iD09p13897>, 1990.

544 Li, S.-M. and Winchester, J.: Aerosol Silicon and Associated Elements in the Arctic High and Mid-Troposphere,
545 *Atmos. Environ.*, 27, 2907-2912, [https://doi.org/10.1016/0960-1686\(93\)90322-P](https://doi.org/10.1016/0960-1686(93)90322-P), 1993.

546 Liggio, J., Li, S.-M., Hayden, K., Taha, Y., Stroud, C., Darlington, A., Drollette, B., Gordon, M., Lee, P., Liu, P.,
547 Leithead, A., Moussa, S., Wang, D., Brien, J., Mittermeier, R., Brook, J., Lu, G., Staebler, R., Han, Y., Tokarek,
548 T., Osthoff, H., Makar, P., Zhang, J., Plata, D., and Gentner, D.: Oil Sands Operations as a Large Source of
549 Secondary Organic Aerosols, *Nature*, 534, 91-94, <https://doi.org/10.1038/nature17646>, 2016.

550 Liu, N., Xu, L., and Cai, Y.: Methyl Siloxanes in Barbershops and Residence Indoor Dust and the Implication for
551 Human Exposures, *Sci. Total. Environ.*, 618, 1324-1330, <https://doi.org/10.1016/j.scitotenv.2017.09.250>, 2018.

552 Mao, J., Ren, X., Brune, W., Olson, J., Crawford, J., Fried, A., Huey, L., Cohen, R., Heikes, B., Singh, H., Blake,
553 D., Sachse, G., Diskin, G., Hall, S., and Shetter, R.: Airborne Measurement of OH Reactivity during INTEX-
554 B, *Atmos. Chem. Phys.*, 9, 163-173, <https://doi.org/10.5194/acp-9-163-2009>, 2009.

555 McFiggans, G., Mentel, T., Wildt, J., Pullinen, I., Kang, S., Kleist, E., Schmitt, S., Springer, M., Tillmann, R., Wu,
556 C., Zhao, D., Hallquist, M., Faxon, C., Breton, M., Hallquist, A., Simpson, D., Bergström, R., Jenkin, M., Ehn,
557 M., Thornton, J., Alfarra, M., Bannan, T., Percival, C., Priestley, M., Topping, D., and Scharr, A.: Secondary
558 Organic Aerosol Reduced by Mixture of Atmospheric Vapours, *Nature*, 565, 587-593,
559 <https://doi.org/10.1038/s41586-018-0871-y>, 2019.

560 Milani, A., Al-Naiema, I., and Stone, E.: Detection of a Secondary Organic Aerosol Tracer Derived from Personal
561 Care Products, *Atmos. Environ.*, 246, <https://doi.org/10.1016/j.atmosenv.2020.118078>, 2021.

562 Ng, N., Kroll, J., Chan, A., Chhabra, P., Flagan, R., and Seinfeld, J.: Secondary Organic Aerosol Formation from
563 m-Xylene, Toluene, and Benzene, *Atmos. Chem. Phys.*, 7, 3909–3922, [https://doi.org/10.5194/acp-7-3909-](https://doi.org/10.5194/acp-7-3909-2007)
564 [2007](https://doi.org/10.5194/acp-7-3909-2007), 2007a.

565 Ng, N., Chhabra, P., Chan, A., Surratt, J., Kroll, J., Kwan, A., McCabe, D., Wennberg, P., Sorooshian, A., Murphy,
566 S., Dalleska, N., Flagan, R., and Seinfeld, J.: Effect of NO_x Level on Secondary Organic Aerosol (SOA)
567 Formation from the Photooxidation of Terpenes, *Atmos. Chem. Phys.*, 7, 5159–5174,
568 <https://doi.org/10.5194/acp-7-5159-2007>, 2007b.

569 Ng, N., Canagaratna, M., Zhang, Q., Jimenez, J., Tian, J., Ulbrich, I., Kroll, J., Docherty, K., Chhabra, P., Bahreini,
570 R., Murphy, S., Seinfeld, J., Hildebrandt, L., Donahue, N., DeCarlo, P., Lanz, V., Prévôt, A., Dinar, E., Rudich,
571 Y., and Worsnop, D.: Organic Aerosol Components Observed in Northern Hemispheric Datasets from Aerosol
572 Mass Spectrometry, *Atmos. Chem. Phys.*, 10, 4625-4641, <https://doi.org/10.5194/acp-10-4625-2010>, 2010.

573 Peng, Z., Taylor, J., Orlando, J., Tyndall, G., and Jimenez, J.: Organic Peroxy Radical Chemistry in Oxidation
574 Flow Reactors and Environmental Chambers and their Atmospheric Relevance, *Atmos. Chem. Phys.*, 19, 813-
575 834, <https://doi.org/10.5194/acp-19-813-2019>, 2019.

576 Peng, Z., Palm, B., Day, D., Talukdar, R., Hu, W., Lambe, A., Brune, W., and Jimenez, J.: Model Evaluation of
577 New Techniques for Maintaining High-NO Conditions in Oxidation Flow Reactors for the Study of OH-
578 Initiated Atmospheric Chemistry, *ACS. Earth. Space. Chem.*, 2, 72-86,
579 <https://doi.org/10.1021/acsearthspacechem.7b00070>, 2017.

580 Pennington, E., Seltzer, K., Murphy, B., Qin, M., Seinfeld, J., and Pye, H.: Modeling Secondary Organic Aerosol
581 Formation from Volatile Chemical Products, *Atmos. Chem. Phys.*, 21, 18247-18261,
582 <https://doi.org/10.5194/acp-21-18247-2021>, 2021.

583 Phares, D., Rhoads, K., Johnston, M., and Wexler, A.: Size-Resolved Ultrafine Particle Composition Analysis 2.
584 Houston, *J. Geophys. Res.*, 108, 1-14, <https://doi.org/10.1029/2001jd001212>, 2003.

585 Presto, A., Hartz, K., and Donahue, N.: Secondary Organic Aerosol Production from Terpene Ozonolysis. 2. Effect
586 of NO_x Concentration, *Environ. Sci. Technol.*, 39, 7046-7054, <https://doi.org/10.1021/es050400s>, 2005.

587 Rauert, C., Shoieb, M., Schuster, J., Eng, A., and Harner, T.: Atmospheric Concentrations and Trends of Poly- and
588 Perfluoroalkyl Substances (PFAS) and Volatile Methyl Siloxanes (VMS) over 7 Years of Sampling in the Global
589 Atmospheric Passive Sampling (GAPS) Network, *Environ. Pollut.*, 238, 94-102,
590 <https://doi.org/10.1016/j.envpol.2018.03.017>, 2018.

591 Rhoads, K., Phares, D., Wexler, A., Johnston, M.: Size-Resolved Ultrafine Particle Composition Analysis 1.
592 Atlanta, *J. Geophys. Res.*, 108, 1-13, <https://doi.org/10.1029/2001jd001211>, 2003.

593 Riipinen, I., Juuti, T., Pierce, J., Petäjä, T., Worsnop, D., Kulmala, M., and Donahue, N.: The Contribution of
594 Organics to Atmospheric Nanoparticle Growth, *Nat. Geosci.*, 5, 453-458, <https://doi.org/10.1038/ngeo1499>,
595 2012.

596 Rücker, C. and Kümmerer, K.: Environmental Chemistry of Organosiloxanes, *Chem. Rev.*, 115, 466-524,
597 <https://doi.org/10.1021/cr500319v>, 2015.

598 Safron, A., Strandell, M., Kierkegaard, A., and Macleod, M.: Rate Constants and Activation Energies for Gas-
599 Phase Reactions of Three Cyclic Volatile Methyl Siloxanes with the Hydroxyl Radical, *Int. J. Chem. Kinet.*, 47,
600 420-428, <https://doi.org/10.1002/kin.20919>, 2015.

601 Sakurai, T., Imaizumi, Y., Kuroda, K., Hayashi, T., and Suzuki, N.: Georeferenced multimedia environmental fate
602 of volatile methylsiloxanes modeled in the populous Tokyo Bay catchment basin, *Sci Total Environ*, 689, 843-
603 853, <https://doi.org/10.1016/j.scitotenv.2019.06.462>, 2019.

604 Sarrafzadeh, M., Wildt, J., Pullinen, I., Springer, M., Kleist, E., Tillmann, R., Schmitt, S., Wu, C., Mentel, T., Zhao,
605 D., Hastie, D., and Scharr, A.: Impact of NO_x and OH on Secondary Organic Aerosol Formation from β-Pinene
606 Photooxidation, *Atmos. Chem. Phys.*, 16, 11237-11248, <https://doi.org/10.5194/acp-16-11237-2016>, 2016.

607 Simonen, P., Saukko, E., Karjalainen, P., Timonen, H., Bloss, M., Saksa, P., Rönkkö, T., Keskinen, J., and Maso,
608 M.: A New Oxidation Flow Reactor for Measuring Secondary Aerosol Formation of Rapidly Changing
609 Emission Sources, *Atmos. Meas. Tech.*, 10, 1519-1537, <https://doi.org/10.5194/amt-10-1519-2017>, 2017.

610 Sommerlade, R., Parlar, H., Wrobel, D., Kochs, P.: Product Analysis and Kinetics of the Gas-Phase Reactions of
611 Selected Organosilicon Compounds with OH Radicals Using a Smog Chamber-Mass Spectrometer System,
612 Environ. Sci. Technol., 27, 2435-2440, <https://doi.org/10.1021/es00048a019>, 1993.

613 Tang, X., Misztal, P., Nazaroff, W., and Goldstein, A.: Siloxanes Are the Most Abundant Volatile Organic
614 Compound Emitted from Engineering Students in a Classroom, Environ. Sci. Technol. Lett., 2, 303-307,
615 <https://doi.org/10.1021/acs.estlett.5b00256>, 2015.

616 Tkacik, D., Lambe, A., Jathar, S., Li, X., Presto, A., Zhao, Y., Blake, D., Meinardi, S., Jayne, J., Croteau, P., and
617 Robinson, A.: Secondary Organic Aerosol Formation from in-Use Motor Vehicle Emissions Using a Potential
618 Aerosol Mass Reactor, Environ. Sci. Technol., 48, 11235-11242, <https://doi.org/10.1021/es502239y>, 2014.

619 Wang, D.-G., Norwood, W., Alaei, M., Byer, J., and Brimble, S.: Review of Recent Advances in Research on the
620 Toxicity, Detection, Occurrence and Fate of Cyclic Volatile Methyl Siloxanes in the Environment, Chemosphere,
621 93, 711-725, <https://doi.org/10.1016/j.chemosphere.2012.10.041>, 2013.

622 Wang, X., Schuster, J., Jones, K., and Gong, P.: Occurrence and Spatial Distribution of Neutral Perfluoroalkyl
623 Substances and Cyclic Volatile Methylsiloxanes in the Atmosphere of the Tibetan Plateau, Atmos. Chem. Phys.,
624 18, 8745-8755, <https://doi.org/10.5194/acp-18-8745-2018>, 2018.

625 Wang, X., Lee, S., Sheng, G., Chan, L., Fu, J., Li, X., Min, Y., and Chan, C.: Cyclic organosilicon compounds in
626 ambient air in Guangzhou, Macau and Nanhai, Pearl River Delta, Appl. Geochemistry, 16, 1447-1454,
627 [https://doi.org/10.1016/S0883-2927\(01\)00044-0](https://doi.org/10.1016/S0883-2927(01)00044-0), 2001.

628 Wildt, J., Mentel, T., Scharr, A., Hoffmann, T., Andres, S., Ehn, M., Kleist, E., Müsgen, P., Rohrer, F., Rudich, Y.,
629 Springer, M., Tillmann, R., and Wahner, A.: Suppression of New Particle Formation from Monoterpene
630 Oxidation by NO_x, Atmos. Chem. Phys., 14, 2789-2804, <https://doi.org/10.5194/acp-14-2789-2014>, 2014.

631 Wu, Y. and Johnston, M.: Molecular Characterization of Secondary Aerosol from Oxidation of Cyclic
632 Methylsiloxanes, J. Am. Soc. Mass Spectrom., 27, 402-409, <https://doi.org/10.1007/s13361-015-1300-1>, 2016.

633 Wu, Y. and Johnston, M.: Aerosol Formation from OH Oxidation of the Volatile Cyclic Methyl Siloxane (cVMS)
634 Decamethylcyclopentasiloxane, Environ. Sci. Technol., 51, 4445-4451,
635 <https://doi.org/10.1021/acs.est.7b00655>, 2017.

636 Xiao, R., Zammit, I., Wei, Z., Hu, W.-P., MacLeod, M., and Spinney, R.: Kinetics and Mechanism of the Oxidation
637 of Cyclic Methylsiloxanes by Hydroxyl Radical in the Gas Phase: An Experimental and Theoretical Study,
638 Environ. Sci. Technol., 49, 13322-13330, <https://doi.org/10.1021/acs.est.5b03744>, 2015.

639 Xu, S., Warner, N., Nizzetto, P., Durham, J., and McNett, D.: Long-Range Transport Potential and Atmospheric

640 Persistence of Cyclic Volatile Methylsiloxanes Based on Global Measurements, *Chemosphere*, 228, 460-468,
641 <https://doi.org/10.1016/j.chemosphere.2019.04.130>, 2019.

642 Zhao, D., Schmitt, S., Wang, M., Acir, I., Tillmann, R., Tan, Z., Novelli, A., Fuchs, H., Pullinen, I., Wegener, R.,
643 Rohrer, F., Wildt, J., Scharr, A., Wahner, A., and Mentel, T.: Effects of NO_x and SO₂ on the Secondary Organic
644 Aerosol Formation from Photooxidation of α -Pinene and Limonene, *Atmos. Chem. Phys.*, 18, 1611-1628,
645 <https://doi.org/10.5194/acp-18-1611-2018>, 2018.

646 Zhou, C., Jang, M., and Yu, Z.: Simulation of SOA Formation from the Photooxidation of Monoalkylbenzenes in
647 the Presence of Aqueous Aerosols Containing Electrolytes under Various NO_x Levels, *Atmos. Chem. Phys.*, 19,
648 5719-5735, <https://doi.org/10.5194/acp-19-5719-2019>, 2019.

649